

# RSC Advances



This is an *Accepted Manuscript*, which has been through the Royal Society of Chemistry peer review process and has been accepted for publication.

*Accepted Manuscripts* are published online shortly after acceptance, before technical editing, formatting and proof reading. Using this free service, authors can make their results available to the community, in citable form, before we publish the edited article. This *Accepted Manuscript* will be replaced by the edited, formatted and paginated article as soon as this is available.

You can find more information about *Accepted Manuscripts* in the [Information for Authors](#).

Please note that technical editing may introduce minor changes to the text and/or graphics, which may alter content. The journal's standard [Terms & Conditions](#) and the [Ethical guidelines](#) still apply. In no event shall the Royal Society of Chemistry be held responsible for any errors or omissions in this *Accepted Manuscript* or any consequences arising from the use of any information it contains.

1 Efficient removal of atrazine in water with Fe<sub>3</sub>O<sub>4</sub>/MWCNTs nanocomposite as a  
2 heterogeneous Fenton-like catalyst

3 Lian Yu<sup>1</sup>, Xiaofang Yang<sup>1</sup>, Yushi Ye<sup>2</sup>, Dongsheng Wang\*<sup>1</sup>

4 <sup>1</sup>State key Laboratory of Environmental Aquatic Chemistry, Research Center for  
5 Eco-Environmental Sciences, Chinese Academy of Sciences, P.O. Box 2871, Beijing  
6 100085, China

7 <sup>2</sup>Changjiang River Scientific Research Institute, Changjiang Water Resources  
8 Commission, Wuhan 430010, China

### 9 **Abstract**

10 Fe<sub>3</sub>O<sub>4</sub> and multi-walled carbon nanotubes hybrid materials (Fe<sub>3</sub>O<sub>4</sub>/MWCNTs)  
11 were synthesized by a coprecipitation combined hydrothermal method. The  
12 nanocomposites were applied for adsorption and degradation of atrazine (ATZ) in the  
13 presence of H<sub>2</sub>O<sub>2</sub>. The obtained catalysts were characterized by TEM, XRD, BET,  
14 XPS and Raman spectroscopy. The effects of solution pH, catalysts dosage, H<sub>2</sub>O<sub>2</sub>  
15 concentration and iron leaching on the degradation of ATZ were investigated.  
16 Fe<sub>3</sub>O<sub>4</sub>/MWCNTs showed a higher utilization efficiency of H<sub>2</sub>O<sub>2</sub>, higher ability of  
17 adsorption for ATZ and higher degradation efficiency of ATZ than Fe<sub>3</sub>O<sub>4</sub>  
18 nanoparticles in the batch degradation experiment. The degradation efficiency  
19 increased with the solution pH decreasing from 8.0 to 3.0. The catalytic results  
20 showed that Fe<sub>3</sub>O<sub>4</sub>/MWCNTs presented good performances for the degradation of  
21 ATZ, achieving 81.4% decomposition of ATZ after 120 min at reaction conditions of  
22 H<sub>2</sub>O<sub>2</sub> concentration 3.0 mmol/L, catalysts dosage 0.1 g/L, ATZ concentration 10.0

23 mg/L, pH 5.0 and T 30°C. Three degradation products (desethylatrazine,  
24 desisopropylatrazine, and 2-hydroxyatrazine) were detected during heterogeneous  
25 Fenton reaction in solution. The stability, reusability of Fe<sub>3</sub>O<sub>4</sub>/MWCNTs for ATZ  
26 degradation were also investigated.

27 **Keywords:** Magnetic carbon nanotube; Heterogeneous Fenton; Fenton; Adsorption;  
28 Atrazine

29

30

## 31 1. Introduction

32 Atrazine (ATZ) (2-chloro-4-(ethylamino))-6-isopropylamino-s-triazine) is widely  
33 used as a herbicide with 70000-90000 tons annually in the world.<sup>[1]</sup> It is extensively  
34 used in agriculture to control broad leaf and grassy weeds in corn, rice, sorghum and  
35 sugarcane fields. Moreover, ATZ is also widely applied to non-agricultural fields such  
36 as lawns and turf. Because of its widespread use, moderate water solubility and high  
37 persistence in water (the half-life of atrazine is as long as about 100 days), ATZ has  
38 been frequently detected in soil and surface waters in North America and Europe,  
39 where it often exceeds the 10 µg/L level of concern for aquatic ecosystems.<sup>[2]</sup>

40 ATZ shows slight toxicity to many fish species, and less toxicity to aquatic  
41 invertebrates.<sup>[2,3]</sup> As a widely used herbicide, ATZ is also highly toxic to algae and  
42 aquatic vascular plants.<sup>[2]</sup> As far as for human health, the main threat related to ATZ  
43 exposure is its endocrine disruption capabilities.<sup>[2,4]</sup> Because of its endocrine  
44 disrupting effect, ATZ is included in the list of prior substances by the European  
45 Union.<sup>[5,6]</sup> Although ATZ has been banned in the European Union, it is still in use in  
46 North America and China. Thus, it is very important to develop efficient methods for  
47 ATZ removal.

48 Traditional physical and chemical methods (coagulation, adsorption, reverse  
49 osmosis, etc.) can generally be used for ATZ removal. Nevertheless, ATZ is usually  
50 non-destructive after being treated with these methods, and the post-treatment of the  
51 adsorbent or the solid wastes is necessary and expensive. Advanced oxidation  
52 processes (AOPs) have been regarded as effective methods to oxidize these

53 compounds, because they can produce hydroxyl radicals ( $\cdot\text{OH}$ ), a powerful  
54 unselective oxidants (2.8 V vs. NHE (pH 0)), which can mineralize almost any  
55 organic pollutant.<sup>[7]</sup> Among the AOPs technologies, Fenton reaction ( $\text{H}_2\text{O}_2 + \text{Fe}^{2+}/\text{Fe}^{3+}$ )  
56 has been proven to be one of the most effective methods to degrade organic pollutants  
57 in wastewater. Unfortunately, there are two critical drawbacks in traditional Fenton  
58 system: (1) Removal of the ferric ions remaining in the treated water complicates the  
59 whole process and makes the method uneconomic and even leads to secondary metal  
60 ion pollution easily. (2) A traditional homogeneous Fenton system works well only  
61 under the highly acidic conditions (pH 2-3).<sup>[8,9]</sup> In order to overcome the  
62 disadvantages of the homogeneous Fenton reaction, the heterogeneous Fenton-like  
63 systems, in which soluble ferric ions are replaced by Fe-containing solids (e.g.,  $\text{Fe}^0$ ,  
64  $\text{Fe}_3\text{O}_4$ ,  $\text{Fe}_2\text{O}_3$ ,  $\text{FeOOH}$ , and so on), have been recently developed.<sup>[10,11]</sup> Especially,  
65 magnetite ( $\text{Fe}_3\text{O}_4$ ) has been reported as an efficient catalyst for heterogeneous  
66 Fenton-like process.<sup>[12-22]</sup> Magnetite exhibits several characteristics that are important  
67 for the Fenton reaction: (1) it contains  $\text{Fe}^{2+}$  that might play an important role as an  
68 electron donor to initiate the Fenton reaction; (2) the octahedral site in the magnetite  
69 structure can easily accommodate both  $\text{Fe}^{2+}$  and  $\text{Fe}^{3+}$ ,  $\text{Fe}^{2+}$  can be reversibly oxidized  
70 and reduced in the same structure; and (3)  $\text{Fe}_3\text{O}_4$  has peroxidase-like activity which  
71 can active  $\text{H}_2\text{O}_2$ .<sup>[12]</sup> The excellent catalytic activity, biocompatibility, easy preparation  
72 and convenient separation from water by external magnetic field, make  $\text{Fe}_3\text{O}_4$  a  
73 promising catalyst for wastewater treatment.

74 However,  $\text{Fe}_3\text{O}_4$  nanoparticles usually aggregate during the reaction process,

75 resulting in reduced catalytic activity.<sup>[15]</sup> So, many efforts have been made to improve  
76 this situation.<sup>[23-26]</sup> Iron oxides can be immobilized on organic or inorganic supports to  
77 form novel heterogeneous Fenton catalysts. Carbon materials such as multiwalled  
78 carbon nanotubes,<sup>[25,27]</sup> graphene,<sup>[28,29]</sup> and activated carbon<sup>[30,31]</sup> have attracted great  
79 attention because of their excellent properties, including acid/base resistance and high  
80 thermal stability. Particularly, due to large reactive area, good dispersion of iron  
81 oxides, and high reaction rate, carbon nanotube-supported iron oxides have attracted  
82 much attention for heterogeneous oxidation of pollutants such as azo dyes and  
83 bisphenol A.<sup>[27,32]</sup> Recently multi-walled carbon nanotube-supported magnetite  
84 ( $\text{Fe}_3\text{O}_4/\text{MWCNT}$ ) has been synthesized and used as the heterogeneous catalyst for  
85 Fenton reaction.<sup>[25,33]</sup>  $\text{Fe}_3\text{O}_4/\text{MWCNTs}$  demonstrated high oxidation efficiency of the  
86 contaminants (i.e., 17 $\alpha$ -methyltestosterone and synthetic dyes) and can be easily  
87 separated from water by external magnetic field after treatment.<sup>[27,33]</sup> Due to the  
88 hydrophobic surface, MWCNTs exhibit strong interactions with organic chemicals.  
89 MWCNTs are an excellent adsorbent for organic contaminants in water treatment  
90 compared with activated carbon and octadecyl adsorbent (C18).<sup>[34]</sup> Consequently,  
91 MWCNTs are an attractive and competitive support compared with other materials for  
92 its adsorption property and stability.<sup>[35]</sup> Hu et al.<sup>[27]</sup> prepared the MWCNTs supported  
93  $\text{Fe}_3\text{O}_4$  nanocomposites by in situ growth. The as-prepared catalyst was used to  
94 degrade 17 $\alpha$ -methyltestosterone with  $\text{H}_2\text{O}_2$  by Fenton reaction. In our study,  
95  $\text{Fe}_3\text{O}_4/\text{MWCNTs}$  catalyst has been prepared by coprecipitation combined with  
96 hydrothermal method. Compared with the catalysts synthesized by in situ growth,

97 Fe<sub>3</sub>O<sub>4</sub>/MWCNTs prepared by coprecipitation combined with hydrothermal method  
98 showed better stability and crystallinity, the morphology of Fe<sub>3</sub>O<sub>4</sub> nanoparticles is  
99 more uniform and Fe<sub>3</sub>O<sub>4</sub> nanoparticles dispersed well on the surface of MWCNTs.  
100 For the first time, the Fe<sub>3</sub>O<sub>4</sub>/MWCNTs catalyst had been used in Fenton reaction to  
101 adsorb and degrade pesticide atrazine in water.

## 102 **2. Experimental**

### 103 2.1 Materials

104 The MWCNTs (diameter, 30-50 nm; length, ~20 μm) used in this work were  
105 purchased from Chengdu Institute of Organic Chemicals, Chinese Academy of  
106 Science. All the other chemicals were analytic grade and used without further  
107 purification. FeCl<sub>3</sub>·6H<sub>2</sub>O, FeCl<sub>2</sub>·4H<sub>2</sub>O, ammonia solution, and H<sub>2</sub>O<sub>2</sub> were purchased  
108 from Beijing Chemical Reagents Company. Atrazine (99.2%) and its degradation  
109 products desethyl-desisopropyl-2-hydroxy-atrazine (99.6%),  
110 desisopropyl-2-hydroxy-atrazine (DIHA, 95.4%), desethyl-2-hydroxy-atrazine  
111 (DEHA, 98.7%), desethyl-desisopropyl-atrazine (DEIA, 98.3%), desethyl-atrazine  
112 (DEA, 99.9%), desisopropyl-atrazine (DIA, 96.1%), 2-hydroxy-atrazine (ATZOH,  
113 94.7%) were purchased from Sigma Aldrich. Tert-Butanol (t-BuOH) was purchased  
114 from Sigma Aldrich (>99.5%). All solutions were prepared in ultra-pure water  
115 (Milli-Q water, Millipore system). Solutions were subject to a brief period in an  
116 ultrasound bath to achieve better dissolution.

### 117 2.2 Catalyst synthesis

118 Purification of MWCNTs:

119 For purification and oxidation the MWCNTs surface to facilitate a uniform  
120  $\text{Fe}_3\text{O}_4$  deposition on their outer walls, 2.0 g of the pristine MWCNTs were dispersed  
121 in 200 ml 68%  $\text{HNO}_3$  by exerting ultrasonic dispersion (Kunshan, KQ-250DE, 50  
122 kHz, 100 W) and refluxed at  $70^\circ\text{C}$  with constant stirring for 14 h. After cooling to  
123 room temperature, the treated MWCNTs were separated from the black suspension  
124 through a vacuum filter, and then washed with deionized (DI) water until pH neutral,  
125 the obtained MWCNTs were dried under vacuum at  $40^\circ\text{C}$ . The dried MWCNTs were  
126 gently milled into powder for use.

127 Preparation of  $\text{Fe}_3\text{O}_4/\text{MWCNTs}$ :

128 A mixture containing 0.14 g  $\text{FeCl}_3 \cdot 6\text{H}_2\text{O}$ , 0.04 g  $\text{FeCl}_2 \cdot 4\text{H}_2\text{O}$ , and 0.10 g  
129 MWCNTs was placed in 160 ml deionized water, vigorously stirred at  $60^\circ\text{C}$  in a  
130 three-neck flask under the purge of nitrogen gas. After the addition of 0.2 ml ammonia  
131 solution and stirred for 30 min, the  $\text{Fe}_3\text{O}_4/\text{MWCNTs}$  colloidal solution was formed.  
132 The obtained MWCNTs colloidal solution was then transferred into a 200 mL  
133 teflon-lined autoclave. The autoclave was sealed and kept at  $120^\circ\text{C}$  for 12 h, then  
134 cooled naturally to room temperature. The precipitate was separated from the  
135 suspension by a magnet, and then washed with DI water to remove the residual  
136 reagents. After repeated washing with DI water and absolute methanol under  
137 ultrasonication for 5 min, the formed  $\text{Fe}_3\text{O}_4/\text{MWCNTs}$  nanocomposites were dried in  
138 a vacuum oven at  $60^\circ\text{C}$  for 24 h. The cleaned MWCNT/ $\text{Fe}_3\text{O}_4$  was used in the  
139 subsequent characterization and application work.

140 2.3 Characterization methods



141 A transmission electron microscope (TEM, JEOL-2010) were employed to  
142 characterize the morphology of the catalysts and the distribution of magnetic  
143 nanoparticles in MWCNTs. The crystalline phase of the synthesized samples were  
144 determined by X-ray diffraction (XRD, Phillips PW 1050-3710 Diffractometer) with  
145 Cu K $\alpha$  radiation ( $\lambda=1.5406 \text{ \AA}$ ). The sample magnetization curves were determined  
146 using a vibrating sample magnetometer (VSM, Quantum Design MPMS-5S). The  
147 surface properties of the catalysts were measured using nitrogen  
148 adsorption-desorption experiments at 77 K. The surface area was calculated using the  
149 standard Brunauer–Emmett–Teller (BET) equation. All of the calculations were  
150 automatically performed using an accelerated surface area and porosimeter system  
151 (ASAP 2010, Micromeritics). X-ray photo-electron spectroscopy (XPS, Al K-Alpha,  
152 Thermo Fisher Scientific) with monochromatic Al K $\alpha$  X-ray radiation at 1486.71 eV  
153 was used to identify metal oxidation states of the nanocomposites. Raman spectra  
154 were recorded with a JY-HR800 (Jobin Yvon) spectrometer equipped with a confocal  
155 microscope.

#### 156 2.4. Degradation of ATZ by heterogeneous Fenton experiments

157 All experiments were conducted in the dark in a 500 mL conical flask (with 200  
158 mL aqueous solution) placed in a thermostated water bath (TZ-2EH) with an agitation  
159 of 150 rpm. The reactions were initiated by adding a desired dosage of H<sub>2</sub>O<sub>2</sub> to a  
160 pH-adjusted solution (by H<sub>2</sub>SO<sub>4</sub> or NaOH) containing Fe<sub>3</sub>O<sub>4</sub>/MWCNTs and atrazine.  
161 The suspension was sampled at predetermined time intervals, meanwhile, 2.0 mL  
162 t-BuOH was added into 2.0 mL sample to quench the reaction. The aqueous phase

163 was sampled for the analysis of pH, the concentrations of ATZ, H<sub>2</sub>O<sub>2</sub>, Fe(II), and total  
164 soluble Fe. The solid catalyst separated from aqueous phase was rinsed by 5 mL  
165 methanol for three times. The rinsed methanol was mixed for analysis. The residual  
166 ATZ amount is the summation of that in aqueous phase and solid phase. As in ATZ  
167 adsorption experiment, the concentration of ATZ is just the ATZ remained in aqueous  
168 phase. The reusability of the catalyst was evaluated by washing the catalyst with  
169 methanol and DI water, drying the used catalyst under vacuum, and using it for the  
170 next reaction under similar experimental conditions. Experiments were carried out at  
171 least in duplicate, and all results were expressed as a mean value. In addition, control  
172 experiments and the effects of pH, initial H<sub>2</sub>O<sub>2</sub> concentration, Fe<sub>3</sub>O<sub>4</sub>/MWCNTs  
173 loading and dissolved iron on ATZ degradation were carried out according to the same  
174 steps as above.

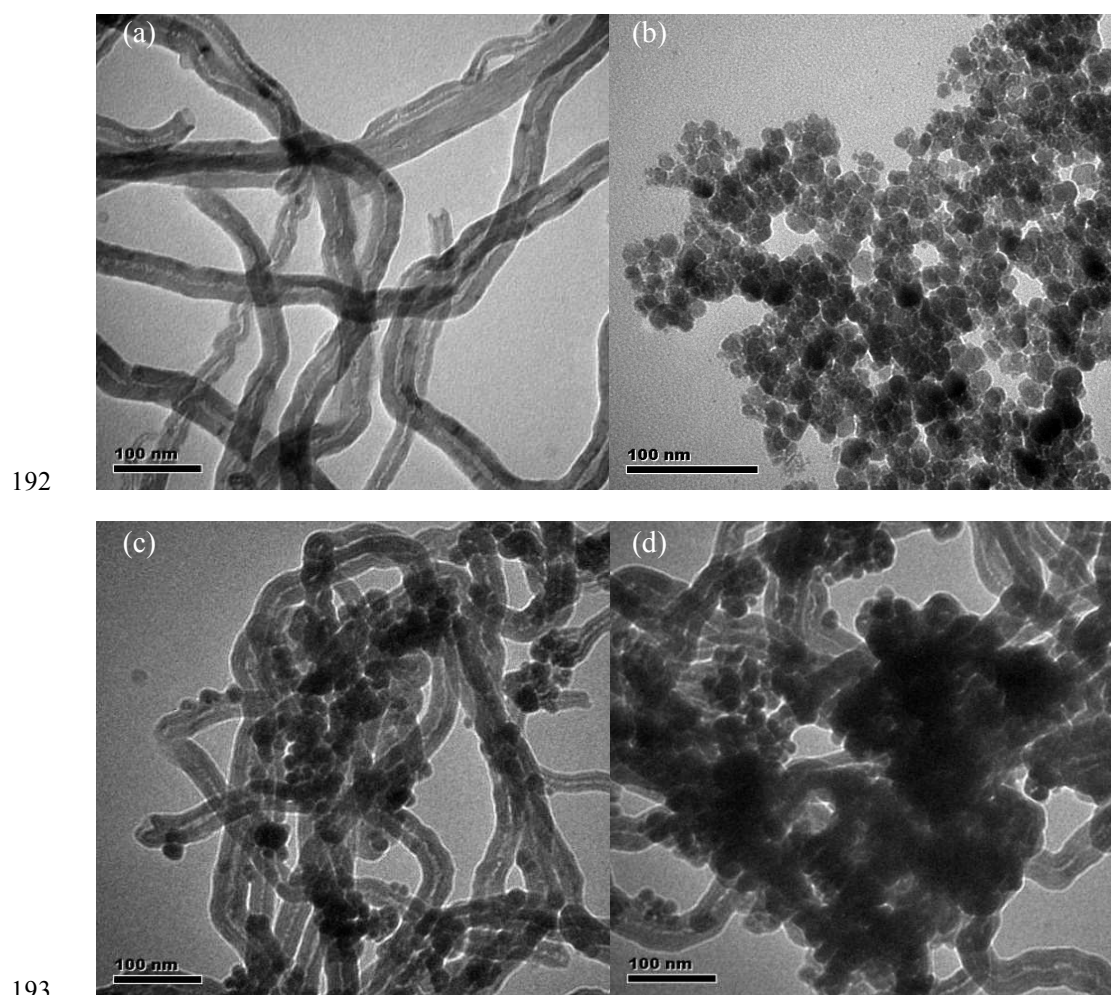
## 175 2.5. Analytic methods

176 Concentration of ATZ and its degradation intermediates was tested by a  
177 high-performance liquid chromatography HPLC equipped with a UV diode array  
178 detector (DAD). Separation was achieved using a Lichrocart C18-RP Purospher Star  
179 (250 mm×4.6 mm, 5µm) column and a water/methanol mobile phase. The mobile  
180 phase flow was 1 ml/min and the composition was gradually changed from 50:50 to  
181 30:70 v/v in 21 min. ATZ concentration was calibrated and measured at 222 nm and  
182 ATZ intermediates at 215 nm. Total organic carbon (TOC) was analyzed using a Multi  
183 TOC/TN Analyzer (2100, Analytik Jena AG Corporation). The solution pH was  
184 measured by a Thermo Orion model 8103BN pH-meter. Ferrous ion and total

185 dissolved iron concentrations were measured according to the 1,10-phenanthroline  
186 method,<sup>[11]</sup> using a UV-VIS spectrophotometer ((UVmini-1240, Shimadzu)) at 510  
187 nm. H<sub>2</sub>O<sub>2</sub> concentration was measured at  $\lambda = 400$  nm with a UV-VIS  
188 spectrophotometer (UVmini-1240, Shimadzu) after adding titanlyl sulfate solution (a  
189 yellow complex is formed).

### 190 3. Results and discussion

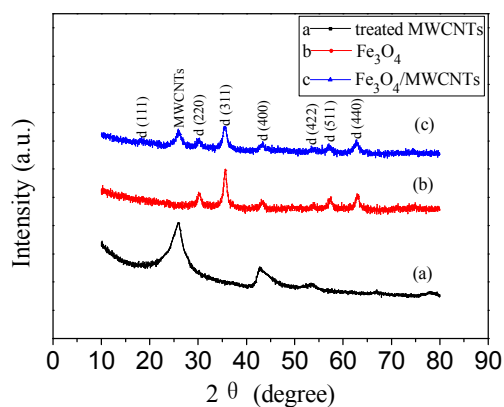
#### 191 3.1. Characterization of catalyst



194 Fig. 1. TEM images of the treated MWCNTs (a), Fe<sub>3</sub>O<sub>4</sub> (b), Fe<sub>3</sub>O<sub>4</sub>/MWCNTs (c) and reused

195 Fe<sub>3</sub>O<sub>4</sub>/MWCNTs (d).

196 It can be seen from Fig. 1a that there was a distortion in the linear structure of  
 197 MWCNTs, indicating that, in some situations, the damage extended beyond the  
 198 outermost graphene sheet and into the underlying sidewalls. Fig. 1b showed that the  
 199 distribution of diameter of the synthesized  $\text{Fe}_3\text{O}_4$  nanoparticles ranging from 10 nm to  
 200 30 nm. As can be seen from Fig. 1c,  $\text{Fe}_3\text{O}_4$  nanoparticles grew regularly on the surface  
 201 of MWCNTs with diameters ranging from 10 to 30 nm. Although the nanocomposites  
 202 had been washed with water and methanol for several times, and underwent  
 203 ultrasonication before TEM measurement, most of the  $\text{Fe}_3\text{O}_4$  nanoparticles were still  
 204 found on MWCNTs surface. This reflected the strong interaction between MWCNTs  
 205 and  $\text{Fe}_3\text{O}_4$  nanoparticles. As can be seen in Fig. 1d, the  $\text{Fe}_3\text{O}_4$  nanoparticles in  
 206  $\text{Fe}_3\text{O}_4/\text{MWCNTs}$  nanocomposites showed some but not serious agglomeration after  
 207 being reused for three times for oxidation reaction.

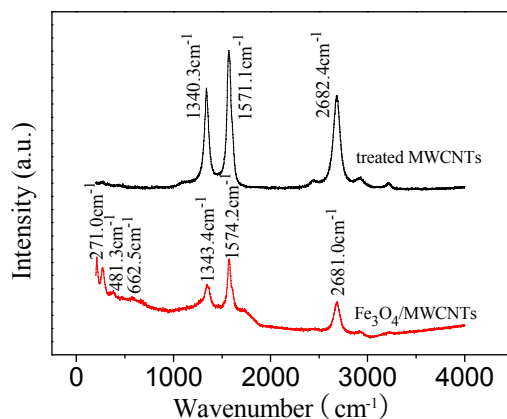


208

209 Fig. 2. X-ray diffraction patterns of MWCNTs (a),  $\text{Fe}_3\text{O}_4$  (b) and  $\text{Fe}_3\text{O}_4/\text{MWCNTs}$  (c).

210 Fig. 2 shows the XRD patterns of MWCNTs,  $\text{Fe}_3\text{O}_4$  nanoparticles and  
 211  $\text{Fe}_3\text{O}_4/\text{MWCNTs}$  nanocomposites. A Diffraction peak at  $2\theta=25.9^\circ$ , which is assigned  
 212 to MWCNTs,<sup>[25]</sup> can be seen for treated MWCNTs and  $\text{Fe}_3\text{O}_4/\text{MWCNTs}$

213 nanocomposites. As shown in Fig. 2b and c, the characteristic peaks for  $\text{Fe}_3\text{O}_4$   
214 ( $2\theta=18.3, 30.3, 35.7, 43.5, 53.4, 57.4, 62.8$  marked by their indices d(111), d(220),  
215 d(311), d(400), d(422), d(511) and d(440)),<sup>[36]</sup> can be observed for the synthesized  
216  $\text{Fe}_3\text{O}_4$  nanoparticles and  $\text{Fe}_3\text{O}_4/\text{MWCNTs}$  nanocomposites. As can be seen from Fig.  
217 2c, the peak at  $2\theta=25.9^\circ$  for  $\text{Fe}_3\text{O}_4/\text{MWCNTs}$  is smaller than that of MWCNTs, this is  
218 because that the MWCNTs content in  $\text{Fe}_3\text{O}_4/\text{MWCNTs}$  is 50 wt%.

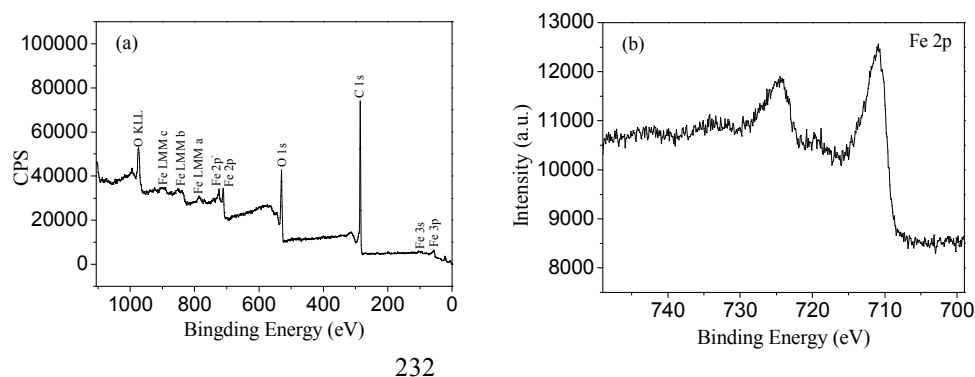


219

220 Fig. 3. Raman spectra of the treated MWCNTs and  $\text{Fe}_3\text{O}_4/\text{MWCNTs}$  nanocomposites.

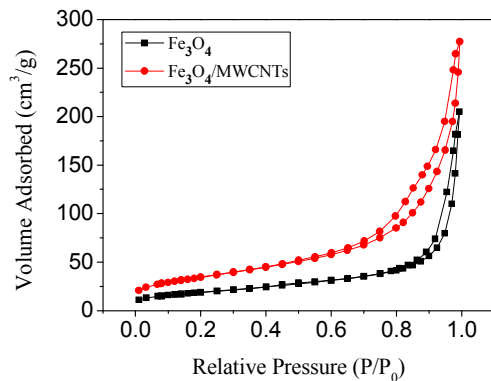
221 Fig. 3 shows the Raman spectrogram of treated MWCNTs and  $\text{Fe}_3\text{O}_4/\text{MWCNTs}$   
222 nanocomposites. As can be seen from Fig. 3, the crystallinity of MWCNTs in treated  
223 MWCNTs and  $\text{Fe}_3\text{O}_4/\text{MWCNTs}$  is different. Some extra peaks in  $\text{Fe}_3\text{O}_4/\text{MWCNTs}$  at  
224 lower wavenumbers ( $271.0, 481.3$  and  $662.5 \text{ cm}^{-1}$ ) can be attributed to the Fe-O bonds  
225 and the Fe-C bonds, confirming that  $\text{Fe}_3\text{O}_4$  nanoparticles were anchored on the  
226 surface of MWCNTs.<sup>[27]</sup> As is known, G ( $1571.1 \text{ cm}^{-1}$ ) band can reflect the purity and  
227 regular structure of MWCNTs, while D band ( $1340.3 \text{ cm}^{-1}$ ) can reflect the defects at  
228 the surface of MWCNTs.<sup>[27]</sup> As can be seen in Fig. 3, the  $I_G/I_D$  ratio of MWCNTs

229 changed from 1.34 to 1.44 after  $\text{Fe}_3\text{O}_4$  loading. The increase of the ratio suggests that  
 230 the atomic ordering of the MWCNTs was enhanced and the structure defects were  
 231 reduced. The peak centered at  $2682.4\text{ cm}^{-1}$  can be assigned to  $D^*$  band of MWCNTs.



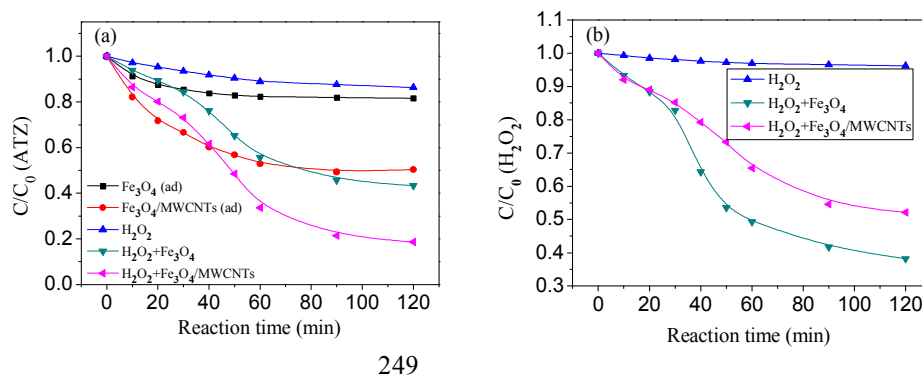
232  
 233 Fig. 4. XPS spectra of the  $\text{Fe}_3\text{O}_4/\text{MWCNTs}$  nanocomposites (a) and high-resolution scan of Fe 2p  
 234 region (b).

235 As shown in Fig. 4a, the peaks at binding energy of 285.1, 530.1 and 711.1 eV  
 236 can be attributed to C 1s, O 1s, and Fe 2p, respectively. There are two peaks at  
 237 binding energies of 710.9 and 725.1 eV for Fe 2p XPS spectrum (Fig. 4b), and  
 238 these can be ascribed to Fe 2p<sub>1/2</sub> and Fe 2p<sub>3/2</sub> respectively. The results are in  
 239 accordance with literature for magnetite<sup>[37]</sup> and agreed with the XRD results.



240  
 241 Fig. 5. Nitrogen adsorption/desorption isotherms for  $\text{Fe}_3\text{O}_4$  and  $\text{Fe}_3\text{O}_4/\text{MWCNTs}$  nanocomposites

242 As can be seen in Fig. 5, N<sub>2</sub> adsorption/desorption isotherms for Fe<sub>3</sub>O<sub>4</sub>  
 243 nanoparticles and Fe<sub>3</sub>O<sub>4</sub>/MWCNTs nanocomposites displayed type  $\square$  isotherms. The  
 244 isotherm of Fe<sub>3</sub>O<sub>4</sub> nanoparticles is below that of Fe<sub>3</sub>O<sub>4</sub>/MWCNTs nanocomposites,  
 245 indicating lower surface area (67.35 m<sup>2</sup>·g<sup>-1</sup> for Fe<sub>3</sub>O<sub>4</sub> nanoparticles, and 112.81 m<sup>2</sup>·g<sup>-1</sup>  
 246 for Fe<sub>3</sub>O<sub>4</sub>/MWCNTs nanocomposites) and pore volume of the former. This can be  
 247 attributed to the porosity of the treated MWCNTs that were used as support.  
 248 3.2. Atrazine degradation experiments by heterogeneous Fenton reaction



250 Fig. 6. Degradation of atrazine (a) and decomposition of H<sub>2</sub>O<sub>2</sub> (b) along with time under different  
 251 conditions. ([ATZ]<sub>0</sub>=10 mg/L; [H<sub>2</sub>O<sub>2</sub>]<sub>0</sub>=3.0 mmol/L; [Fe<sub>3</sub>O<sub>4</sub>]=0.1 g/L; [Fe<sub>3</sub>O<sub>4</sub>/MWCNTs]=0.1  
 252 g/L; pH 5.0; T=30°C.)

253 Fig. 6 shows the ATZ degradation (a) and H<sub>2</sub>O<sub>2</sub> decomposition (b) with time  
 254 under different experimental conditions. As shown in Fig. 6a, the adsorption processes  
 255 proceed very quickly, and the equilibrium concentrations are reached in about 60 min  
 256 for Fe<sub>3</sub>O<sub>4</sub> and Fe<sub>3</sub>O<sub>4</sub>/MWCNTs. The percentages of adsorbed ATZ were 18.4% and  
 257 49.6% respectively for Fe<sub>3</sub>O<sub>4</sub> and Fe<sub>3</sub>O<sub>4</sub>/MWCNTs. As can be seen in Fig. 6a, little  
 258 ATZ was degraded in the presence of H<sub>2</sub>O<sub>2</sub> only, this can be ascribed to the low  
 259 oxidation potential of H<sub>2</sub>O<sub>2</sub> compared with hydroxyl and perhydroxyl radicals. In the

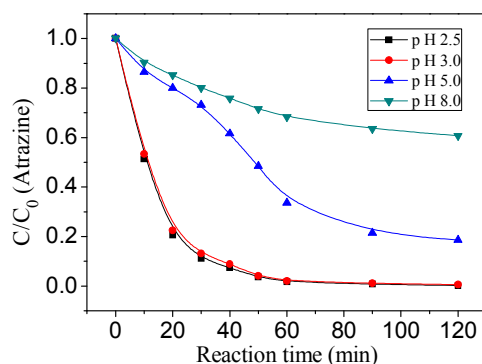


260 presence of  $\text{H}_2\text{O}_2$  and  $\text{Fe}_3\text{O}_4/\text{MWCNTs}$ , a conversion efficiency of 81.4% for ATZ can  
261 be achieved after 120 min reaction. There are two stages in the heterogeneous Fenton  
262 reaction: induction period and rapid degradation stage, the degradation rates were  
263 accelerated after reaction for about 30 minutes. As can be seen from Fig. 6a,  
264  $\text{Fe}_3\text{O}_4/\text{MWCNTs}$  were much more efficient than  $\text{Fe}_3\text{O}_4$  nanoparticles. Some  
265 researchers found that activated carbon and graphite could generate free radicals such  
266 as superoxide ion and activate hydrogen peroxide, Carbon materials have been used in  
267 heterogeneous Fenton reactions.<sup>[38,39]</sup> But Hu et al.<sup>[27]</sup> reported that the contribution of  
268 direct catalysis of MWCNTs in  $\text{Fe}_3\text{O}_4/\text{MWCNTs}$  to the improved degradation  
269 performance was very limited.

270 As shown in Fig. 6b,  $\text{H}_2\text{O}_2$  was not converted without the presence of catalysts.  
271 In the presence of  $\text{Fe}_3\text{O}_4$  and  $\text{Fe}_3\text{O}_4/\text{MWCNTs}$ , 61.8% and 47.9%  $\text{H}_2\text{O}_2$  were  
272 decomposed in 120 min, respectively. Taking the degradation efficiencies of ATZ into  
273 consideration,  $\text{Fe}_3\text{O}_4/\text{MWCNTs}$  showed higher utilization efficiency of  $\text{H}_2\text{O}_2$  than  
274  $\text{Fe}_3\text{O}_4$  nanoparticles. It can be deduced that the adsorbed ATZ molecules which were  
275 closed to Fe-ions immobilized on WMCNTs, were easily attacked by the  
276 produced  $\cdot\text{OH}$ . The synergistic effect resulting from the adsorption performance of  
277 MWCNTs caused the different degradation efficiency.

278 3.3. Effect of pH





279

280 Fig. 7. The effect of pH on ATZ degradation. ( $[\text{ATZ}]_0=10$  mg/L;  $[\text{H}_2\text{O}_2]_0=3.0$  mmol/L;

281

$[\text{Fe}_3\text{O}_4/\text{MWCNTs}] = 0.1$  g/L;  $T=30^\circ\text{C}$ .)

282

The experiments were carried out under four different pH values of 2.5, 3.0, 5.0

283

and 8.0. It can be seen from Fig. 7 that solution pH has a crucial influence on the

284

removal of ATZ by Fenton-like reaction, lower pH was beneficial for the degradation

285

of ATZ. At pH near neutrality (pH=5.0),  $\text{Fe}_3\text{O}_4/\text{MWCNTs}$  are still active but the ATZ

286

removal efficiency decreased to 81.4%. At pH=8.0, the reaction rate was very slow

287

and 39.7% ATZ can be removed in 120 min. This phenomenon is consistent with

288

other iron oxide based heterogeneous Fenton systems.<sup>[40]</sup> As can be seen, when

289

solution  $\text{pH} \leq 3.0$ , the reaction follows a pseudo-first order law, this is because

290

homogeneous Fenton reaction may take place in the acidic conditions ( $\text{Fe}_3\text{O}_4$

291

nanoparticles dissolved). The existence of high catalytic activity near neutral pH,

292

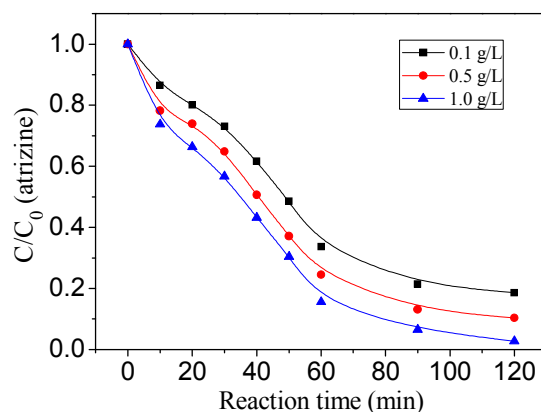
allows these catalysts to be applied at neutral pH, which is impossible for

293

homogeneous Fenton catalysts.

294

3.4. Effect of the catalyst dosage



295

296 Fig. 8. The effect of catalyst dosage on ATZ degradation. ( $[\text{ATZ}]_0=10 \text{ mg/L}$ ;  $[\text{H}_2\text{O}_2]_0=3.0 \text{ mmol/L}$ ;

297

pH 5.0;  $T=30^\circ\text{C}$ .)

298

Fig. 8 shows the influence of the catalyst dosage on the heterogeneous Fenton

299

degradation of ATZ by  $\text{Fe}_3\text{O}_4/\text{MWCNTs}$ . The degradation efficiency increased from

300

81.4% to 97.3% as the catalyst concentration increased from 0.1 g/L to 1.0 g/L. The

301

increased efficiency was mainly due to the increased active sites when more catalyst

302

was added to the solution, and more active sites is favorable for generating more

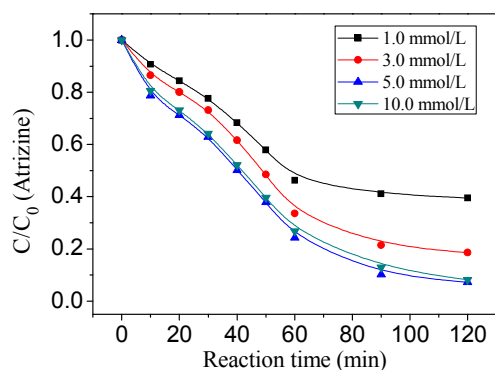
303

free-radical species which can promote the degradation reaction. A catalyst dosage of

304

1.0 g/L led to ATZ being almost completely degraded within 120 min.

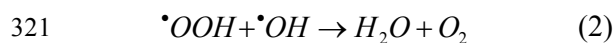
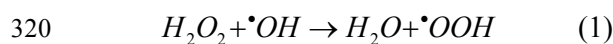
305

3.5. Effect of  $\text{H}_2\text{O}_2$  concentration

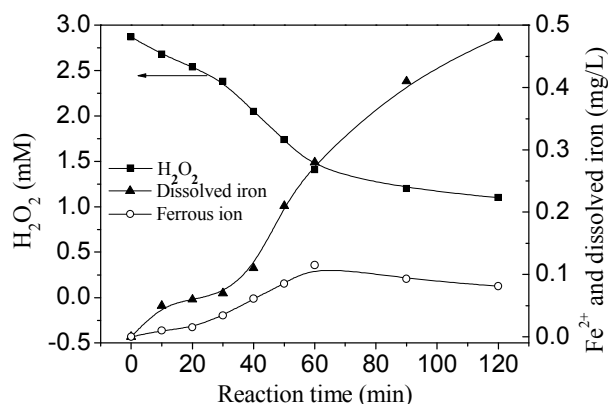
306

307 Fig. 9. The effect of H<sub>2</sub>O<sub>2</sub> dosage on ATZ degradation. ([ATZ]<sub>0</sub>=10 mg/L; [Fe<sub>3</sub>O<sub>4</sub>/MWCNTs] =0.1  
 308 g/L; pH 5.0; T=30°C.)

309 The influence of H<sub>2</sub>O<sub>2</sub> concentration on the degradation of ATZ was illustrated in  
 310 Fig. 9. The degradation efficiency increased from 60.5% to 92.7% when H<sub>2</sub>O<sub>2</sub>  
 311 concentration increased from 1.0 mmol/L to 10.0 mmol/L. At lower concentrations of  
 312 H<sub>2</sub>O<sub>2</sub>, an adequate number of ·OH radicals can not generate, and this slowed the  
 313 oxidation rate and further reduced the removal efficiency. However, when the  
 314 concentration of H<sub>2</sub>O<sub>2</sub> increased to 10.0 mmol/L, a significant improvement did not  
 315 appeared. There are two main disadvantages for using high concentrations of H<sub>2</sub>O<sub>2</sub>.  
 316 First, as H<sub>2</sub>O<sub>2</sub> was excess to the pollutant, the excess H<sub>2</sub>O<sub>2</sub> would not have enough  
 317 substrate to act upon, most of H<sub>2</sub>O<sub>2</sub> would therefore be wasted. Second, higher  
 318 concentrations of H<sub>2</sub>O<sub>2</sub> can result in the scavenging of ·OH radicals (eqs 1 and 2).<sup>[23]</sup>  
 319 Therefore, the concentration of H<sub>2</sub>O<sub>2</sub> should maintain at its optimal level.



322 3.6. Iron leaching

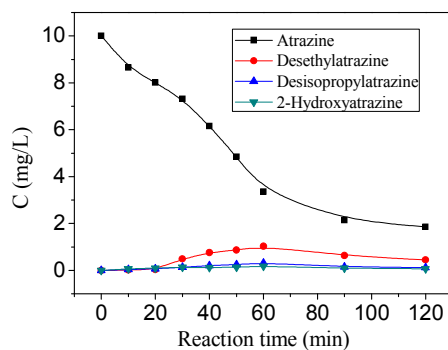


323

324 Fig. 10. Investigation of iron dissolution during ATZ degradation. ( $[\text{ATZ}]_0=10$  mg/L;  $[\text{H}_2\text{O}_2]_0=3.0$   
 325 mmol/L;  $[\text{Fe}_3\text{O}_4/\text{MWCNTs}]=0.1$  g/L; pH 3.0;  $T=30^\circ\text{C}$ .)

326 As can be seen in Fig. 10, the Fe ions concentration during ATZ degradation  
 327 were investigated. As can be seen,  $\text{Fe}_3\text{O}_4$  nanoparticles in  $\text{Fe}_3\text{O}_4/\text{MWCNTs}$  dissolved  
 328 gradually in the solution during the reaction, the concentration of the total dissolved  
 329 iron increased to 0.48 mg/L after 120 min. This demonstrated that homogeneous  
 330 Fenton reaction occurred during ATZ degradation in the bulk solution. As ferrous ions  
 331 can be oxidated to ferric ions by the remaining oxidants (such as  $\cdot\text{OH}$  and  $\text{H}_2\text{O}_2$ ) in the  
 332 solution, the concentration of ferrous reached a peak value at 60 min, and then  
 333 decreased to 0.081 mg/L after 120 min of reaction.

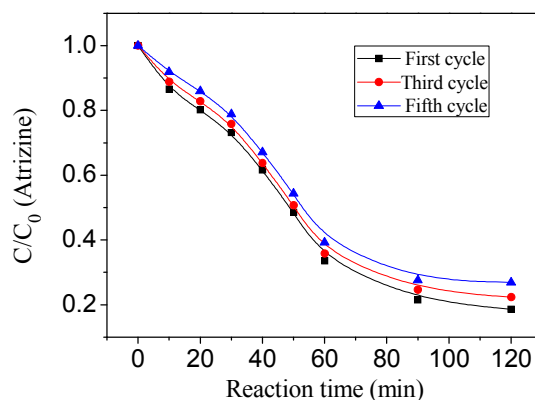
### 334 3.7. Oxidation products



335  
 336 Fig. 11. Variation of the concentration of degradation intermediates detected by HPLC equipped  
 337 with a UV DAD. ( $[\text{ATZ}]_0=10$  mg/L;  $[\text{H}_2\text{O}_2]_0=3.0$  mmol/L;  $[\text{Fe}_3\text{O}_4/\text{MWCNTs}]=0.1$  g/L; pH 5.0;  
 338  $T=30^\circ\text{C}$ .)

339 At the solution pH 5.0, the leaching of iron ions can be ignored, heterogeneous  
 340 Fenton reaction plays the dominant role, the reaction mainly proceed in the surface of  
 341  $\text{Fe}_3\text{O}_4/\text{MWCNTs}$ . MWCNTs are excellent adsorbent for ATZ, ATZ molecules

342 adsorbed by MWCNTs were closed to Fe-ions immobilized on WMCNTs, they were  
343 easily attacked by the produced  $\cdot\text{OH}$ , so  $\text{Fe}_3\text{O}_4/\text{MWCNTs}$  show excellent catalytic  
344 activity. The intermediates derived from ATZ decomposition were analyzed by HPLC.  
345 As can be seen from Fig. 11, the main intermediates were DEA, DIA, ATZ-OH (also  
346 some unidentified oxidation products). The concentration of the intermediates  
347 increased slowly at first 30 min, reached peak values at about 60 min, and then  
348 decreased in the next 60 min. Barreiro et al.<sup>[41]</sup> studied the mechanisms of the ATZ  
349 oxidation in solution by Fenton reaction. They found that it was  $\cdot\text{OH}$  that initiated the  
350 oxidation of ATZ, the oxidation could be initiated through dealkylation (alkylic  
351 sidechain cleavage), alkylic-oxidation (alkylamino side-chain oxidation), and/or  
352 dechlorination (hydroxylation at the chlorine site), and hence the related intermediates  
353 were observed in the present study.<sup>[41]</sup>  
354 3.8 Catalytic stability of  $\text{Fe}_3\text{O}_4/\text{MWCNTs}$



355  
356 Fig. 12. The catalytic activity of reused  $\text{Fe}_3\text{O}_4/\text{MWCNTs}$  on ATZ degradation. ( $[\text{ATZ}]_0=10$  mg/L;  
357  $[\text{H}_2\text{O}_2]_0=3.0$  mmol/L;  $[\text{Fe}_3\text{O}_4/\text{MWCNTs}] =0.1$  g/L; pH 5.0;  $T=30^\circ\text{C}$ .)

358 Successive experiments were carried out to evaluate the stability of the catalyst.

359 From Fig. 12, it can be seen that the activity decreased gradually during three  
360 consecutive runs. The loss of activity can be attributed to the dissolution of  $\text{Fe}_3\text{O}_4$   
361 nanoparticles from the surface of the catalyst as described in section 3.6. In addition,  
362 the agglomeration of  $\text{Fe}_3\text{O}_4$  nanoparticles in the reused  $\text{Fe}_3\text{O}_4/\text{MWCNTs}$  (as can be  
363 seen from TEM patterns of Fig. 1d) can also lead to the decrease of the catalytic  
364 activity of  $\text{Fe}_3\text{O}_4/\text{MWCNTs}$ .

#### 365 **4. Conclusions**

366  $\text{Fe}_3\text{O}_4/\text{MWCNTs}$  nanocomposites were successfully synthesized by  
367 coprecipitation and hydrothermal method.  $\text{Fe}_3\text{O}_4/\text{MWCNTs}$  showed a strong ability  
368 for the adsorption of ATZ in aqueous solution.  $\text{Fe}_3\text{O}_4/\text{MWCNTs}$  can be used as an  
369 efficient heterogeneous Fenton-like catalyst to degrade ATZ in aqueous solution. The  
370 degradation efficiency strongly depends on the solution pH with a sharp increase in  
371 oxidation rate from pH 5.0 to 3.0 which is the pH range where  $\text{Fe}_3\text{O}_4$  dissolution is  
372 strongly increased, and the soluble  $\text{Fe}(\text{II})$  and  $\text{Fe}(\text{III})$  species in solution initiate the  
373 homogeneous Fenton reaction. ATZ removal efficiencies are found not to increase  
374 much with the increasing concentrations of  $\text{Fe}_3\text{O}_4/\text{MWCNTs}$ .  $\text{Fe}_3\text{O}_4/\text{MWCNTs}$   
375 showed higher utilization efficiency of  $\text{H}_2\text{O}_2$  than  $\text{Fe}_3\text{O}_4$  nanoparticles. The enhanced  
376 catalytic activity of  $\text{Fe}_3\text{O}_4/\text{MWCNTs}$  in heterogeneous Fenton system could be  
377 attributed to the well dispersion of  $\text{Fe}_3\text{O}_4$  nanoparticles on MWCNTs, positive effect  
378 of MWCNTs via adsorption of pollutant molecules.

#### 379 **Acknowledgements**

380 This work has been supported by National Nature Science Foundation of China

381 (Grant No. 51338010, 21107125 and 51221892), National Basic Research Program of  
382 China (973 Program, Grant No. 2011CB933704), and the National Natural Science  
383 Funds for Distinguished Yong Scholar (Grant No. 51025830).

384

385 **References**

- 386 [1] M. Graymore, F. Stagnitti and G. Allinson, *Environ. Int.*, 2001, 26, 483.
- 387 [2] US Environmental Protection Agency,  
388 [http://www.epa.gov/opp00001/reregistration/atrazine/atrazine\\_update.htm](http://www.epa.gov/opp00001/reregistration/atrazine/atrazine_update.htm), last  
389 accessed November 2012.
- 390 [3] C. Brassard, L. Gill, A. Stavola, J. Lin and L. Turner, US EPA Policy and  
391 Regulatory Services Branch and Environmental Field Branch, 2003, p. 25.
- 392 [4] A. L. Forgacs, Q. Ding, R. G. Jaremba, I. T. Huhtaniemi, N. A. Rahman and T. R.  
393 Zacharewski, *Toxicol. Sci.*, 2012, 127, 391.
- 394 [5] A. S. Friedmann, *Reprod. Toxicol.*, 2002, 16, 275.
- 395 [6] R. Renner, *Environ. Sci. Technol.*, 2002, 36, 55A.
- 396 [7] C. Comninellis, A. Kapalka, S. Malato, S. A. Parsons, I. Poullos and D.  
397 Mantzavinos, *J. Chem. Technol. Biotechnol.*, 2008, 83, 769.
- 398 [8] G. K. Zhang, Y. Y. Gao, Y. L. Zhang and Y. D. Guo, *Environ. Sci. Technol.*, 2010,  
399 44, 6384.
- 400 [9] Z. H. Ai, L. R. Lu, J. P. Li, L. Z. Zhang, J. R. Qiu and M. H. Wu, *J. Phys. Chem. C*,  
401 2007, 111, 7430.
- 402 [10] W. Wang, Y. Liu, T. L. Li and M. H. Zhou, *Chem. Eng. J.*, 2014, 242, 1.
- 403 [11] L. J. Xu and J. L. Wang, *Appl. Catal. B: Environ.*, 2012, 123, 117.
- 404 [12] L. W. Hou, Q. H. Zhang, F. Jérôme, D. Duprez, H. Zhang and S. Royer, *Appl.*  
405 *Catal. B: Environ.*, 2014, 144, 739.
- 406 [13] R. X. Huang, Z. Q. Fang, X. M. Yan and W. Cheng, *Chem. Eng. J.*, 2012, 197,



- 407 242.
- 408 [14] S. Shin, H. Yoon and J. Jang, *Catal. Commun.*, 2008, 10, 178.
- 409 [15] S. X. Zhang, X. L. Zhao, H. Y. Niu, Y. L. Shi, Y. Q. Cai and G. B. Jiang, J.  
410 *Hazard. Mater.*, 2009, 167, 560.
- 411 [16] S. P. Sun and A. T. Lemley, *J. Mol. Catal. A: Chem.*, 2011, 349, 71.
- 412 [17] J. B. Zhang, J. Zhuang, L. Z. Gao, Y. Zhang, N. Gu, J. Feng, D. L. Yang, J. D.  
413 Zhu and X. Y. Yan, *Chemosphere*, 2008, 73, 1524.
- 414 [18] X. F. Xue, K. Hanna and N. S. Deng, *J. Hazard. Mater.*, 2009, 166, 407.
- 415 [19] K. Rusevova, F. D. Kopinke and A. Georgi, *J. Hazard. Mater.*, 2012, 241, 433.
- 416 [20] M. Usman, P. Faure, C. Ruby and K. Hanna, *Appl. Catal. B: Environ.*, 2012, 117,  
417 10.
- 418 [21] R. C. C. Costa, F. C. C. Moura, J. D. Ardisson, J. D. Fabris and R. M. Lago, *Appl.*  
419 *Catal. B: Environ.*, 2008, 83, 131.
- 420 [22] L. J. Xu and J. L. Wang, *Environ. Sci. Technol.*, 2012, 46, 10145.
- 421 [23] L. C. Zhou, Y. M. Shao, J. R. Liu, Z. F. Ye, H. Zhang, J. J. Ma, Y. Jia, W. J. Gao  
422 and Y. F. Li, *ACS Appl. Mater. Interfaces*, 2014, 6, 7275.
- 423 [24] J. Y. Chun, H. S. Lee, S. H. Lee, S. W. Hong, J. S. Lee, C. H. Lee and J. W. Lee,  
424 *Chemosphere*, 2012, 89, 1230.
- 425 [25] X. B. Hu, Y. H. Deng, Z. Q. Gao, B. Z. Liu and C. Sun, *Appl. Catal. B: Environ.*,  
426 2012, 127, 167.
- 427 [26] L. R. Kong, X. F. Lu, X. J. Bian, W. J. Zhang and C. Wang, *ACS Appl. Mater.*  
428 *Interfaces*, 2011, 3, 35.

- 429 [27] X. B. Hu, B. Z. Liu, Y. H. Deng, H. Z. Chen, S. Luo, C. Sun, P. Yang and S. G.  
430 Yang, *Appl. Catal. B: Environ.*, 2011, 107, 274.
- 431 [28] W. Liu, J. Qian, K. Wang, H. Xu, D. Jiang, Q. Liu, X. W. Yang and H. M. Li, J.  
432 *Inorg. Organomet. Polym.*, 2013, 23, 907.
- 433 [29] S. Guo, G. K. Zhang, Y. D. Guo and J. C. Yu, *Carbon*, 2013, 60, 437.
- 434 [30] L. Gu, N. W. Zhu, H. Q. Guo, S. Q. Huang, Z. Y. Lou and H. P. Yuan, *J. Hazard.*  
435 *Mater.*, 2013, 246, 145.
- 436 [31] H. Y. Zhao, Y. J. Wang, Y. B. Wang, T. C. Cao and G. H. Zhao, *Appl. Catal. B:*  
437 *Environ.*, 2012, 125, 120.
- 438 [32] V. Cleveland, J. P. Bingham and E. Kan, *Sep. Purif. Technol.*, 2014, 133, 388.
- 439 [33] J. H. Deng, X. H. Wen and Q. N. Wang, *Mater. Res. Bull.*, 2012, 47, 3369.
- 440 [34] B. Pan and B. S. Xing, *Environ. Sci. Technol.*, 2008, 42, 9005.
- 441 [35] R. Gonzalez-Olmos, U. Roland, H. Toufar, F. D. Kopinke and A. Georgi, *Appl.*  
442 *Catal. B: Environ.*, 2009, 89, 356.
- 443 [36] Y. Liu, W. Jiang, Y. Wang, X. J. Zhang, D. Song and F. S. Li, *J. Magn. Magn.*  
444 *Mater.*, 2009, 321, 408.
- 445 [37] D. Wilson and M. A. Langell, *Appl. Surf. Sci.*, 2014, 303, 6.
- 446 [38] F. J. Maldonado-Hodar, L. M. Madeira and M. F. Portela, *Appl. Catal. A: Gen.*,  
447 1999, 178, 49.
- 448 [39] F. Lücking, H. Köer, M. Jank and A. Ritter, *Water Res.*, 1998, 32, 2607.
- 449 [40] J. Y. Feng, X. J. Hu and P. L. Yue, *Water Res.*, 2006, 40, 641.
- 450 [41] J. C. Barreiro, M. D. Capelato, L. Martin-Neto and H. C. B. Hansen, *Water Res.*,

451 2007, 41, 55.